Antiswarming: Structure and dynamics of repulsive chemically active particles

Wen Yan and John F. Brady

Phys. Rev. E **96**, 060601 — Published 1 December 2017

DOI: 10.1103/PhysRevE.96.060601

Anti-Swarming: Structure and Dynamics of Repulsive Chemically Active Particles

Wen Yan[1, *] and John F. Brady[2, †]

[1]*Department of Mechanical & Civil Engineering, Division of Engineering & Applied Science, California Institute of Technology*[‡]

[2]*Division of Chemistry & Chemical Engineering and Division of Engineering & Applied Science California Institute of Technology*

(Dated: November 5, 2017)

Chemically active Brownian particles with surface catalytic reactions may repel each other due to diffusiophoretic interactions in the reaction and product concentration fields. The system behavior can be described by a 'chemical' coupling parameter Γ_c that compares the strength of diffusiophoretic repulsion to Brownian motion, and by a mapping to the classical electrostatic One Component Plasma (OCP) system. When confined to a constant-volume domain, Body-Centered Cubic crystals spontaneously form from random initial configurations when the repulsion is strong enough to overcome Brownian motion. Face-Centered Cubic crystals may also be stable. The 'melting point' of the 'liquid-to-crystal transition' occurs at $\Gamma_c \approx 140$ for both BCC and FCC lattices.

I. INTRODUCTION

Chemically active particles suspended in fluids may achieve self-propulsion by surface catalytic reactions of chemical solutes [1]. One mechanism is self-diffusiophoresis, whereby the motion of a particle arises from the asymmetric solute concentration field $c(\boldsymbol{x},t)$ created near its surface. Typically, reactants are consumed on the surface of a chemically active particle, and when a second particle appears is in the vicinity, it is attracted by a diffusiophoretic velocity $\boldsymbol{U} \sim -\nabla c$. Active particles with attractive interactions are observed to exhibit dynamic clustering and gas-liquid phase transition [2–4]. Thermodynamic-like theories [5] utilizing the swim pressure [6] as an equation of state, and other theories based on similar thermodynamic-like models [7–9] work well in describing the phase separation phenomena.

However, few studies have investigated active particles with repulsive interactions. If the surface chemical reactions release solutes instead of consuming them, the solute concentration $c(\boldsymbol{x},t)$ is increased in the vicinity of each particle, and the diffusiophoretic velocity is now repulsive between particles (c.g Fig. 1). Repulsive particles, if confined in a constant volume container, may overcome the randomizing thermal Brownian motion and form a crystal lattice [10]. Derjaguin and Golovanov [11] observed the formation of periodic crystal-like structures in living cells and suggested that it is due to repulsive diffusiophoretic interactions.

A classical example of repulsive particles that show a liquid-to-crystal transition is the so-called One Component Plasma (OCP). In an OCP moving positive charges are immersed in a uniform and neutralizing background sea of negative electrons, and the system behavior is governed by an electrostatic coupling parameter Γ_e, which measures the electrostatic energy relative to thermal energy [12]. It is well known that the liquid-like structure at small Γ_e transforms to BCC (body-centered cubic) for $\Gamma_e \gtrsim 175$ [13–22].

In this work we explore the collective motion of repulsive active particles by simulations with a full solution of the diffusiophoretic interactions as described in our methods paper [23]. We show that repulsive chemically active particles exhibits a 'liquid-to-crystal' phase transition, similar to an OCP. Quantitatively, we define a chemical coupling parameter Γ_c for the chemically active system in analogy to Γ_e for an OCP.

II. PROBLEM FORMULATION

A first order surface catalytic reaction $R \to \theta P$ is assumed to occur homogeneously on the spherical particle surface as illustrated in Fig. 1. Making use of the stoichiometry/diffusivity factor $(1-\theta D_R/D_P)$, the reaction can be taken to be irreversible: $\boldsymbol{j}_R \cdot \boldsymbol{n} = -\kappa c(\boldsymbol{n})$ on the boundary, where c is the reactant concentration, κ is the reaction rate constant and $\boldsymbol{n}$ is the surface normal vector pointing outward from the particle. Here, θ is the stoichiometry of the reaction and D_R and D_P are the diffusivities of the reactants and products, respectively. The Damkhöler number $\mathrm{Da} = a\kappa/D_R$ governs the reaction rate: $\mathrm{Da} \to \infty$ corresponds to diffusion limited due to a fast reaction, while $\mathrm{Da} \to 0$ is the slow reaction-rate limit.

When the chemical solutes are much smaller in size than the active particles, each chemically active particle is driven by the osmotic pressure of the reactant solute concentration $k_BTc(\boldsymbol{x},t)$ integrated over the particle's surface [24, 25] and achieves the velocity

$$\boldsymbol{U}_0 = -(1-\theta D_R/D_P)\frac{L(\Delta)}{6\pi\eta a}\oint \boldsymbol{n}\, k_BTc(\boldsymbol{x},t)dS\,, \quad (1)$$

where a is the particle radius, η is the solution viscosity, and the nondimensional hydrodynamic mobility function $L(\Delta) = (3/2)\Delta^2(1+\frac{2}{3}\Delta)/(1+\Delta)^3$, with $\Delta = \delta/a$,

* wyan@flatironinstitute.org

† jfbrady@caltech.edu

‡ Current Address: Center for Computational Biology, Flatiron Institute, Simons Foundation

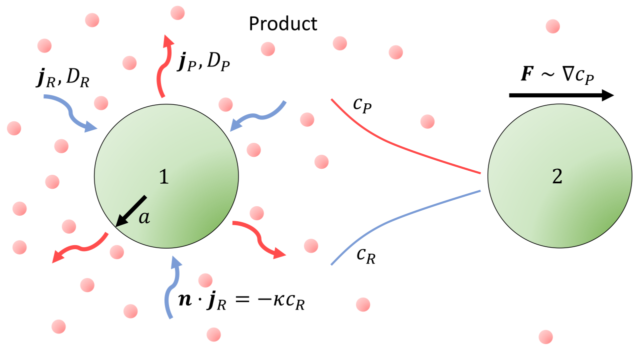

FIG. 1. A schematic for the repulsive diffusiophoretic interaction. Reactant solutes with diffusivity D_R and flux $\boldsymbol{j}_R$ are consumed on the surface of catalytic particle 1 with the first-order boundary condition $\boldsymbol{n} \cdot \boldsymbol{j}_R = -\kappa c_R$. Product solutes (small red dots) leave the particle surface with flux $\boldsymbol{j}_P$ and diffusivity D_P. In the vicinity of the particle 1 c_P is increased while c_R is decreased. When the product is more effective at pushing particle 2 (which occurs when $1-\theta D_R/D_P < 0$) particle 2 feels a repulsive diffusiophoretic force $\boldsymbol{F} \sim \nabla c_P$. From the reaction boundary conditions a simple scaling between c_R and c_P holds [24] and only the reaction concentration field needs to be computed, which we denote simply as c. The particles then move according to (1).

measures the flow of fluid with viscosity η in a layer of thickness δ adjacent to the colloidal particle where the particle-solute interactive force is operative. Here we have taken the simplest form of interactive force between the solute and the colloidal particle, namely a hard-sphere repulsive force at a distance $r_c = a + \delta$ (and δ need not be small compared to the particle size a, although typically it is so). More general interactive forces will only have a quantitative effect and the details are discussed in [25]. The prefactor $(1-\theta D_R/D_P)$ scales the solution of reactant concentration $c(\boldsymbol{x}, t)$ to the total solute concentration of both reactant and products. When $\theta D_R/D_P > 1$, the products push the particles more effectively than the reactants and the particles can be considered sources releasing products and therefore they repel each other. Here in (1) we also assumed that $\Delta = \delta/a$ is the same for both reactant and product solutes. If $\delta_R \neq \delta_P$, the function $L(\Delta)$ could be absorbed into the scale factor, and the new scale factor could be written as $L(\Delta_R) - L(\Delta_P)\theta D_R/D_P$.

The governing equation for $c(\boldsymbol{x}, t)$ is the classic convection-reaction-diffusion equation. The convection is controlled by the Péclet number $\mathrm{Pe} = U_0 a/D_R$. In diffusiophoresis, the particle velocity U_0 is usually so small that $\mathrm{Pe} \ll 1$ [24], and therefore the convection of c can be ignored. Diffusion of the reactive solute is fast enough for c to achieve a steady state, instantaneously following the particle motion. In this case, the governing equation for the reactant reduces to Laplace's equation, $\nabla^2 c = 0$, similar to an electrostatic field. To leading order, the disturbance to the solute concentration field induced by one reactive particle is $c' \sim q/r$, where q is the particle reactivity—that is, how many molecules are consumed on the particle surface in unit time, which is analogous to the electrostatic charge Ze.

The active particles are assumed to be confined in a constant volume three dimensional space, and the reactant is assumed to be released by distributed sources throughout the space to maintain the system as 'chemically neutral.' Therefore the volume average reactant concentration is maintained at a constant $\langle c \rangle$. Without the chemically neutralizing condition, the particles eventually consume all the reactant and no steady state can be achieved. Experimentally, Theurkauff *et al.* [2] have demonstrated a 2D implementation of a chemically neutral suspension in which the solute diffuses into a colloid monolayer reaction zone from a large reservoir and the system is kept evolving for many hours to reach a steady state. The chemically neutral assumption is also common for 3D reactive suspension systems [26].

An analogy to an OCP can be made. The repulsive active particles resemble the positive ions in an OCP, and the chemically neutralizing sources are similar to the electrostatically neutralizing background. By analogy, active particles should be liquid-like when the repulsion is weak and be solid-like when the repulsion is strong enough to order the particles into a periodic lattice.

A key difference, however, is that moving ions in an OCP are point charges and the charges are fixed at Ze, while the reactivity q of a chemically active particle changes in response to the local concentration of reactants due to the chemical reaction on the particle's surface. Also, the reactivity has a distribution on the particle's spherical surface—the particle is more than merely a 'point charge.' The changing reactivity results in changing interactions, which is fundamentally different from the additive pairwise potential assumption employed in previous simulation work on attractive active particles [4, 27]. The changing reactivity also poses a difficulty for thermodynamic-like treatments. Even if we define a mean-field effective pairwise potential, it is state-dependent, and it is known that some thermodynamic inconsistencies and peculiarities may appear for density-dependent pairwise interactions [28, 29].

In this work, we simulate the system with the Accelerated Laplacian Dynamics method [23], which we describe briefly without going into the mathematical details. The chemical reaction on each particle is represented by a multipole expansion, keeping only the monopole, q, and the dipole $\boldsymbol{S}$, similar to electrostatics. Here, q is the net consumption rate of reactant and $\boldsymbol{S}$ is the asymmetry of the consumption on the particle surface. Second, the perturbation c' of each particle to the average field $\langle c \rangle$ is calculated from q, which propagates as $1/r$, and $\boldsymbol{S}$, which propagates as $1/r^2$. Third, with the first order reaction condition, the monopole and dipole strength of particle α follow from a Faxen-type law: $q_\alpha \propto \langle c \rangle + c'(\boldsymbol{x}_\alpha)$, and $\boldsymbol{S}_\alpha \propto \nabla c'(\boldsymbol{x}_\alpha)$, where $c'(\boldsymbol{x}_\alpha)$ and $\nabla c'(\boldsymbol{x}_\alpha)$ are perturbations arising from all particles $\beta \neq \alpha$ and are evaluated at the center of α. (For chemically neutral systems $\nabla \langle c \rangle = 0$.) In this way, the equations for the solute field c are closed and can be solved iteratively at each timestep for different configurations of the active particles.

The diffusiophoretic velocity of an active particle is then determined from the solution for the solute concentration field c at each timestep. The velocity $\boldsymbol{U}_{0,\alpha}$ of particle α in (1) can be calculated analytically utilizing the first-order reaction boundary condition, $\boldsymbol{j}_R \cdot \boldsymbol{n} = -\kappa c(\boldsymbol{n})$, to give

$$\frac{\boldsymbol{U}_{0,\alpha}}{D/a} = -\left(1 - \theta D_R/D_P\right) L(\Delta) \langle c \rangle a^3 \frac{4\pi a \nabla c(\boldsymbol{x}_\alpha)}{(Da+2)\langle c \rangle}. \quad (2)$$

By the assumed uniformity of the reaction on a particle surface there is no self-diffusiophoretic motion; particle motion arises solely from normal diffusiophoresis in the concentration gradient created by the other particles.

The system dynamics are integrated with over-damped Brownian dynamics: $\Delta X = \boldsymbol{U}_0 \Delta t + \Delta X^B + \Delta X^{HS}$, where ΔX^B is the translational Brownian motion satisfying $\langle \Delta X^B \rangle = 0, \langle \Delta X^B \Delta X^B \rangle = 2D\Delta t$, and ΔX^{HS} is the non-overlapping hard-sphere collision displacement calculated with the potential-free algorithm [30].

We nondimensionalize the system with the active particle radius a, the particle diffusion time $\tau_D = a^2/D$, where D is the Brownian diffusivity of an active particle, $D = k_BT/6\pi\eta a$, and the imposed reactant concentration $\langle c \rangle$. The phoretic velocity then behaves as $\boldsymbol{U}_0 \propto -S_D \nabla (c/\langle c \rangle)$, where $S_D = (1 - \theta D_R/D_P) L(\Delta) \langle c \rangle a^3$ is the nondimensional concentration, i.e., the 'fuel concentration.' Increasing $|S_D|$ is equivalent to increasing the hydrogen peroxide concentration in the experiments [2, 31]. In this work, we report only the result of the repulsive case $S_D < 0$. The attractive case for $S_D > 0$ is discussed elsewhere [32].

III. THE WEAK REPULSION REGIME: FLUCTUATING INTERACTIONS

In simulations covering a wide range of volume fraction $0.001 < \phi < 0.15$ and Damköhler number $0.1 < \mathrm{Da} < 10$, we found that under weak repulsion (small $|S_D|$), the system remains randomly distributed due to Brownian motion. To analyze the structure Voronoi cells are built around each particle and the local volume fraction is defined as $\phi_p = \frac{4}{3}\pi a^3/V_p$, where V_p is the volume of the Voronoi cell occupied by that particle.

The first order reaction $R \to \theta P$ gives an infinitely dilute reactivity $q_0 = -4\pi D_R a \langle c \rangle \mathrm{Da}/(1+\mathrm{Da})$. With increasing ϕ, many-body interactions increase the reactivity of a particle and the average reactivity $\langle q \rangle$ increases [26]. In this work we assume that the volumetric average of reactant solute concentration is held constant at $\langle c \rangle$ by the distributed source of reactant, and therefore on average $\langle q \rangle / q_0 > 1$ as shown in Fig. 2. Although in principle $\langle q \rangle / q_0$ should depend on the specific microstructure, the dependence is very weak [33], especially in the regime

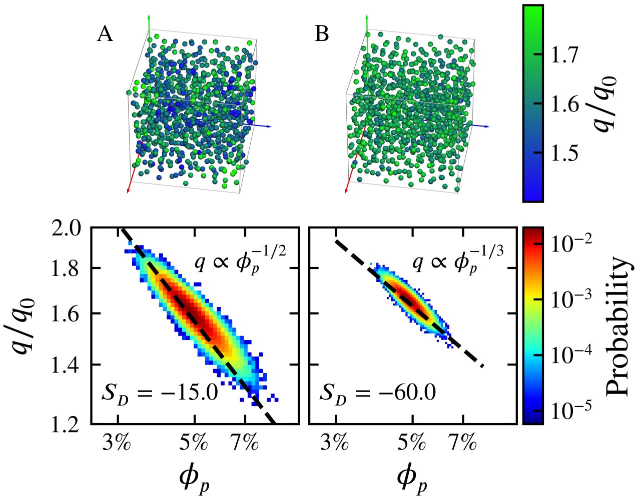

FIG. 2. The distribution of particle reaction q and local volume fraction ϕ_p, and their correlation. A: The snapshot of the equilibrium structure of system in a periodic box of $42a \times 42a \times 42a$, with $\phi = 0.0488$, $\mathrm{Da} = 2.0$, $N = 864$, $S_D = -15.0, \Gamma_c \approx 20$. Each particle is colored by q/q_0. B: The same system, but equilibrated with stronger repulsion $S_D = -60.0, \Gamma_c \approx 80$.

where ϕ is far from the closed-packing limit $\phi_{RCP} \approx 0.64$. The following equation was found to be a universal fit to $\langle q \rangle / q_0$ for all structures and all (Da, ϕ) ranges investigated in this work

$$\frac{\langle q \rangle}{q_0} = \frac{1}{1 - B\phi^{1/3}\mathrm{Da}/(1+\mathrm{Da})}, \quad (3)$$

with $B = 1.62$.

Although on average particles are always supplied with reactant as the global average $\langle c \rangle$ is held constant, locally they still compete for reactant due to the fluctuations of the microstructure. If the local particle volume fraction ϕ is higher than the average $\langle \phi \rangle$, the competition for reactant solutes occurs locally and decreases q of particles with high ϕ_p. We quantify this local competition by the correlation between the single particle reactivity q and the local volume fraction ϕ_p. Fig. 2 shows this correlation for an example system of $\mathrm{Da} = 2, \phi = 0.0488$, at different repulsion strengths. Fig. 2 A and B both show a power-law correlation between q/q_0 and ϕ_p. It is known that the correlation is $q/q_0 \propto \phi_p^{-1/2}$ in random suspensions but changes to $q/q_0 \propto \phi_p^{-1/3}$ in periodic suspensions [34]. The simulation results agree with this transition. These correlations of $\phi_p^{-1/3}$ and $\phi_p^{-1/2}$ are for local fluctuations only, and are not the same as the scaling in (3), which is for the global average of q over all particles in the system. With $S_D = -15$ in Fig. 2 A the structure remains random and the correlation follows $q/q_0 \propto \phi_p^{-1/2}$. Under strong repulsion ($S_D = -60$ in Fig. 2 B), the particle reactivity q is narrowly distributed around $\langle q \rangle$, because the strong repulsion keeps the particles almost homogeneously distributed. In this case each particle experiences almost the same microstructure, and the structure is close to a periodic configuration. Thus the correlation in this case is close to $q/q_0 \propto \phi_p^{-1/3}$.

Therefore, in the strong repulsion case, we can ignore the fluctuations in q and define a parameter based on $\langle q \rangle$ to quantify the leading order effect of repulsion vs Brownian motion, again by an analogy to an OCP. In an OCP, the controlling parameter is $\Gamma_e = (Ze)^2/(4\pi\epsilon_0 L k_B T)$, where Ze is the ion charge, ϵ_0 is the dielectric permittivity, and L is a length scale determined by ion number density n: $L = (4\pi n/3)^{-1/3}$. The parameter Γ_e measures the ratio of the electrostatic potential energy of two ions separated by L to the thermal energy $k_B T$. Similarly, we can define Γ_c as the ratio of diffusiophoretic repulsion to Brownian motion, where the subscript c denotes chemically active particles. To leading order, the repulsive diffusiophoretic velocity $U_0 \sim -S_D \nabla c$, as shown in (2), and in the over-damped limit $\boldsymbol{F} \propto 6\pi\eta a U_0 \sim \nabla(1/r)$. Thus, we can define an 'average potential of chemical force' Φ_c according to $\boldsymbol{F} = -\nabla \Phi_c$. We use the same length scale $L = (4\pi n/3)^{-1/3} = \phi^{-1/3} a$ as in an OCP, but replace the number density n with particle volume fraction ϕ, since particles are not point charges. We also scale $\langle q \rangle$ with q_0, as in the scaling relation (3). Therefore, we have $\Phi_L = S_D k_B T \langle q \rangle / [(\mathrm{Da}+2)\langle c \rangle D_R L]$, and Γ_c can be defined in the nondimensional form:

$$\Gamma_c = -4\pi \frac{\mathrm{Da}}{1+\mathrm{Da}} \frac{S_D}{\mathrm{Da}+2} \phi^{1/3} \frac{\langle q \rangle}{q_0} . \tag{4}$$

Note, the thermal energy $k_B T$ does not appear in Γ_c because both the repulsive force (in equation (1)) and thermal Brownian motion scale linearly with $k_B T$.

IV. THE STRONG REPULSION REGIME: 'LIQUID-TO-CRYSTAL' PHASE TRANSITION

The analogy to an OCP and the similar definition of Γ_c implies the existence of a liquid-to-crystal phase transition, which is confirmed by our simulations.

In an OCP, BCC is considered the stable crystal structure. However, the free energy difference between BCC and FCC is very small, and FCC can also maintain its structure, similar to diamond and graphite. The melting point of both FCC and BCC are reported [35, 36] to be: $\Gamma_e^{BCC} \approx 175$ and $\Gamma_e^{FCC} \approx 185$, respectively.

For chemically active particles, we conducted simulations in 3D cubic periodic boxes with approximately $N = 1000$ particles, with large S_D ($\Gamma_c \sim 800$), starting from a random particle distribution and tracked the structural evolution for a long time $\sim 1000\tau_D$. The simulation process is equivalent to suddenly cooling a liquid to very low temperature and allowing it to relax to equilibrium. BCC crystals formed in all 'cooling' simulations, with inevitable distortion and defects. The formation of a BCC lattice is similar to the experiments [19] and simulations [22] of an OCP.

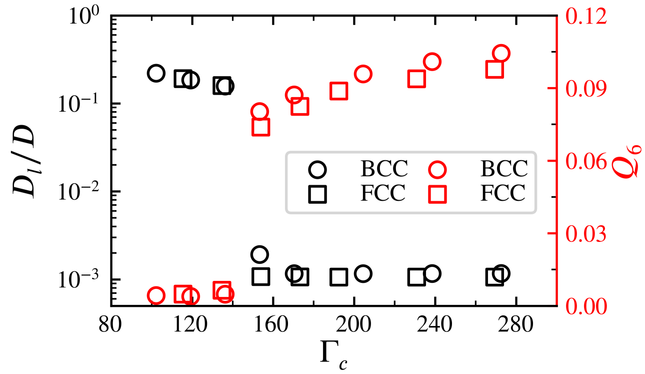

FIG. 3. The measurement of structural change of BCC and FCC crystals, both for Da = 2.0. $\phi = 0.0388$ for BCC system and $\phi = 0.0488$ for FCC system.

In order to accurately locate the transition, i.e., the 'melting point' of the repulsive active particle crystal, 'melting simulations' were conducted. Melting, instead of cooling, is chosen because in the liquid-solid phase transition the cooling process usually requires a large amount of sub-cooling to provide the crystallization with enough 'driving force', while melting usually occurs immediately at the melting point. Although the thermal energy $k_B T$ cancels out in the definition of Γ_c, increasing the Brownian motion is equivalent to increasing the 'temperature' and corresponds to decreasing Γ_c. We start from 3D periodic systems of perfect crystal structures and run simulations covering a wide range of Γ_c, for sufficiently long times $\sim 1000\tau_D$.

To quantify the structure we use both the dynamic criterion D_l/D [37], where D_l is the long-time diffusivity of the particles, and the static order parameter Q_6 [38]. As shown in Figs. 3 and 4, D_l/D and Q_6 give consistent results in quantifying the system 'melting point', for both BCC and FCC structures. However, the calculation of D_l/D requires significant computation time because we must track the system for a very long time. Thus, we use Q_6 when mapping the entire phase diagram for the range of $0.001 < \phi < 0.15$, $0.1 < \mathrm{Da} < 10$, and $N \approx 1000$. When calculating Q_6 we include approximately the second shell of neighbors [38]. Including only the first shell results in a smaller value of Q_6, but the measured transition point does not change. Test runs show that a simple cubic lattice spontaneously transforms to a distorted BCC lattice. Therefore we search for the melting point of BCC and FCC lattices only.

As shown in Fig. 4, all the melting simulations show the same sharp jump in Q_6, and the transition point for both BCC and FCC is $\Gamma_c^{BCC,FCC} \approx 140$. Two movies can be found in the Supplemental Material [39], illustrating the freezing and melting processes.

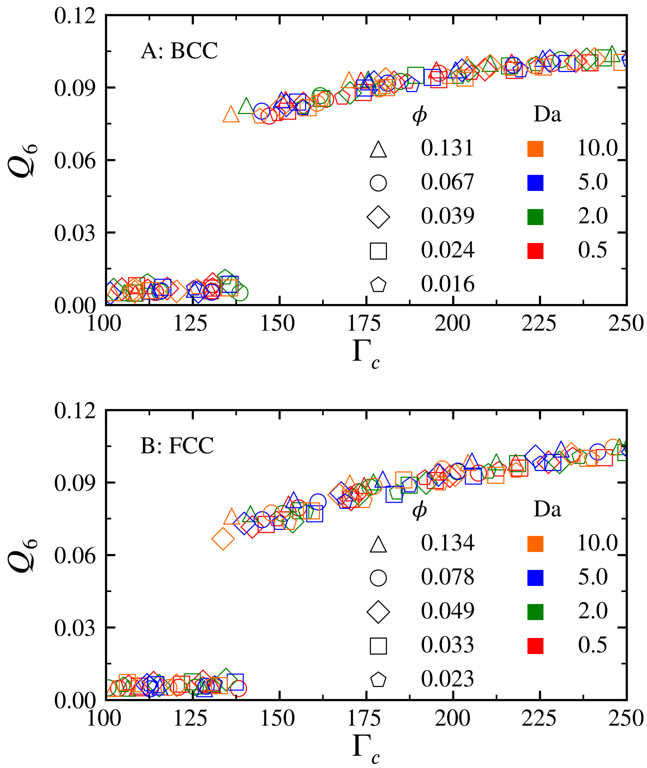

FIG. 4. The measurement Q_6 of the melting process. A: The initial configuration is BCC and B: The initial configuration is FCC. For each combination of ϕ (shape) and Da (color), simulations of different S_D are conducted so that a range of $100 < \Gamma_c < 250$ is covered. The melting point for both BCC and FCC is $\Gamma_c \approx 140$.

V. CONCLUSIONS & DISCUSSION

We explored repulsive chemically active particles with simulations and showed that the system behavior can be determined by a single parameter Γ_c. The 'liquid-to-crystal' phase transition is located at $\Gamma_c^{BCC,FCC} \approx 140$, which differs from the OCP results $\Gamma_e^{BCC} \approx 175, \Gamma_e^{FCC} \approx 185$. The difference may come from three effects. First, although for repulsive chemically active particles the almost homogeneous local structure allows us to define Γ_c based on $\langle q \rangle$, fluctuations in q are still present, which is very different from an OCP system with fixed point charges. More importantly, the changing reactivity leads to Brinkman screening [40], which changes the long-ranged $1/r$ interaction to a screened $\exp(r/L_B)/r$, where $L_B \sim a\phi^{-1/2}$ is the screening length. The role of screening in repulsive active matter is a complicated issue and it is unclear whether it causes the differences in the melting point of Γ_c compared to Γ_e. Second, limited by computing resources, in simulations we truncated the particle multipole expansion at the dipole level, and so some inaccuracy is inevitable. Third, the transition point of an OCP system is typically found by searching for the free energy cross-over via Monte-Carlo methods. However, thermodynamics for repulsive active particles are not yet defined, and so we have to search for a transition point with dynamic simulations, which may give $\sim 10\%$ error depending on the system property and methodology [41].

Regarding the experimental realizations with hydrogen peroxide and oxygen molecules as the fuel, both are at the nanoscale, and in this limit $L(\Delta)a^3 \sim \delta^2 a$, where $\delta \sim 10^{-9}$m. Therefore, $S_D \sim O(100)$ for $\langle c \rangle \sim 1\mathrm{mol\,L^{-1}}$, and $\Gamma_c \sim O(100)$. So the estimated phase-transition at $\Gamma_c^{BCC,FCC} \sim 140$ is within the reach of the experiments. If the particles are confined to a monolayer by gravity and geometry, similar repulsive crystals should form, which should be hexagonal because the repulsion to leading order is isotropic. It would be interesting to see if our predictions are borne out by experiment.

In this work we investigated homogeneously reactive particles. In addition to particle-particle interaction, active Janus particle with a reactive hemisphere also achieve self-propulsion given by (1). For Janus particles no repulsive crystal formation is observed in simulations, because Janus particles can achieve a much larger velocity, $\boldsymbol{U}_0$, so the long-ranged repulsion due to diffusiophoresis is not strong enough to trap them in a lattice. Also, it is not legitimate to define a Γ_c^J by simply replacing the translational diffusivity $D = k_B T/\zeta$ with the swim-diffusivity D^{swim} for Janus particles and then determine the system dynamics with Γ_c^J, because D^{swim} only appears at a time scale longer than the reorientation time τ_R, and the short-time dynamics are important in many cases, such as crystal formation. In fact, it is not clear whether a meaningful parameter Γ_c^J can be defined for Janus particles. Moreover, while the swim pressure and thermodynamic-like theories [5, 6] describe attractive active swimmer behaviors well, it is not clear whether a similar non-equilibrium thermodynamic argument can be conducted to estimate the melting point, $\Gamma_c^{BCC,FCC}$, of repulsive swimmers. Repulsive Janus particles are left for a future study.

ACKNOWLEDGMENTS

We thank Prof. Zhen-Gang Wang for bringing our attention to the repulsive system. This work is supported by NSF CBET-1437570.

[1] S. J. Ebbens and J. R. Howse, Soft Matter **6**, 726 (2010).
[2] I. Theurkauff, C. Cottin-Bizonne, J. Palacci, C. Ybert, and L. Bocquet, Phys. Rev. Lett. **108**, 268303 (2012).
[3] I. Buttinoni, J. Bialké, F. Kümmel, H. Löwen,

C. Bechinger, and T. Speck, Phys. Rev. Lett. **110**, 238301 (2013).
[4] J. Palacci, S. Sacanna, A. P. Steinberg, D. J. Pine, and P. M. Chaikin, Science **339**, 936 (2013).
[5] S. C. Takatori and J. F. Brady, Phys. Rev. E **91**, 032117 (2015).
[6] S. C. Takatori, W. Yan, and J. F. Brady, Phys. Rev. Lett. **113**, 028103 (2014).
[7] J. Stenhammar, A. Tiribocchi, R. J. Allen, D. Marenduzzo, and M. E. Cates, Phys. Rev. Lett. **111**, 145702 (2013).
[8] A. P. Solon, Y. Fily, A. Baskaran, M. E. Cates, Y. Kafri, M. Kardar, and J. Tailleur, Nat. Phys. **11**, 673 (2015).
[9] M. E. Cates and J. Tailleur, Annu. Rev. Condens. Matter Phys. **6**, 219 (2015).
[10] S. Soh, K. J. M. Bishop, and B. A. Grzybowski, J. Phys. Chem. B **112**, 10848 (2008).
[11] B. Derjaguin and M. Golovanov, Colloids and Surfaces **10**, 77 (1984).
[12] S. G. Brush, H. L. Sahlin, and E. Teller, J. Chem. Phys. **45**, 2102 (1966).
[13] M. J. Gillan, J. Phys. C **7**, L1 (1974).
[14] F. J. Rogers, Phys. Rev. A **10**, 2441 (1974).
[15] D. Stroud and N. Ashcroft, Phys. Rev. A **13**, 1660 (1976).
[16] N. Itoh and S. Ichimaru, Phys. Rev. A **16**, 2178 (1977).
[17] B. Bernu, J. Stat. Phys. **21**, 447 (1979).
[18] M. Baus and J. P. Hansen, Phys. Rep. **59**, 1 (1980).
[19] J. N. Tan, J. J. Bollinger, B. Jelenkovic, and D. J. Wineland, Phys. Rev. Lett. **75**, 4198 (1995).
[20] H. DeWitt, W. Slattery, D. Baiko, and D. Yakovlev, Contrib. Plasma Phys. **41**, 251 (2001).
[21] A. I. Chugunov, D. A. Baiko, D. G. Yakovlev, H. E. De Witt, and W. L. Slattery, Physica A **323**, 413 (2003).
[22] J. Daligault, Phys. Rev. E **73**, 056407 (2006).
[23] W. Yan and J. F. Brady, The Journal of Chemical Physics **145**, 134902 (2016).
[24] U. M. Córdova-Figueroa and J. F. Brady, Phys. Rev. Lett. **100**, 158303 (2008).
[25] J. F. Brady, J. Fluid Mech. **667**, 216 (2011).
[26] R. T. Bonnecaze and J. F. Brady, P. Roy. Soc. Lond. A Mat. **432**, 445 (1991).
[27] G. S. Redner, A. Baskaran, and M. F. Hagan, Phys. Rev. E **88**, 012305 (2013).
[28] A. A. Louis, J. Phys. Condens. Matter **14**, 9187 (2002).
[29] C. F. Tejero and M. Baus, J. Chem. Phys. **118**, 892 (2003).
[30] D. R. Foss and J. F. Brady, J. Rheol. **44**, 629 (2000).
[31] J. R. Howse, R. A. L. Jones, A. J. Ryan, T. Gough, R. Vafabakhsh, and R. Golestanian, Phys. Rev. Lett. **99**, 048102 (2007).
[32] W. Yan, *Dynamics of chemically active suspensions*, PhD Thesis, California Institute of Technology (2016).
[33] J. R. Lebenhaft and R. Kapral, J. Stat. Phys. **20**, 25 (1979).
[34] R. T. Bonnecaze and J. F. Brady, J. Chem. Phys. **94**, 537 (1991).
[35] D. H. E. Dubin, Phys. Rev. A **42**, 4972 (1990).
[36] G. S. Stringfellow, H. E. DeWitt, and W. L. Slattery, Phys. Rev. A **41**, 1105 (1990).
[37] H. Löwen, T. Palberg, and R. Simon, Phys. Rev. Lett. **70**, 1557 (1993).
[38] P. R. ten Wolde, M. J. Ruiz-Montero, and D. Frenkel, Phys. Rev. Lett. **75**, 2714 (1995).
[39] "See Supplemental Material at [ ] for the freezing process generated between $t = 400\tau_D$ and $500\tau_D$ from a simulation with $N = 864, \phi = 13.4\%, \mathrm{Da} = 2, S_D = 90, \Gamma_c \approx 220$. See Supplemental Material at [ ] for the melting process generated from a simulation with $N = 686, \phi = 6.7\%, \mathrm{Da} = 5, S_D = 84, \Gamma_c \approx 110$.".
[40] J. F. Morris and J. F. Brady, Ind. Eng. Chem. Res. **34**, 3514 (1995).
[41] G. P. Hoffmann and H. Löwen, J. Phys. Condens. Matter **13**, 9197 (2001).